Quaternary Science Reviews 351 (2025) 109185

Contents lists available at ScienceDirect

Quaternary Science Reviews

journal homepage: www.elsevier.com/locate/quascirev

High-resolution sedimentary record in the eastern Mediterranean shelf shows reduced Nile-derived mud after the Little Ice Age (1830 CE)

Yael Edelman-Furstenberg [a,*], Navot Morag [a], Henko C. de Stigter [b], Onn Crouvi [a], Nadya Teutsch [a], Orit Hyams-Kaphzan [a]

[a] Geological Survey of Israel, Yeshayahu Leibowitz 32, Jerusalem, 9692100, Israel
[b] NIOZ Royal Netherlands Institute for Sea Research, Department of Ocean Systems, Texel, the Netherlands

A R T I C L E I N F O

Handling Editor: Giovanni Zanchetta

Keywords:
^{210}Pb sediment age
Little Ice age (LIA)
Nile river sediments
Sahara derived sediments
Benthic foraminifera
Aswan high dam

A B S T R A C T

Chemical, sedimentological and micropaleontological records were used to track recent climatic and ecological events recorded in eastern Mediterranean shelf sediments. By studying a high-resolution record of well-dated sediment from the Israeli shelf, natural and anthropogenic influence during the past 270 years were differentiated and pinpointed to major events.

The most prominent changes occurred in sediment source at the end of the Little Ice Age (LIA), in 1830–1840 CE. Coarse, quartzose sand comprised only 5% of the sediment during the LIA, and increased significantly after the LIA to levels of up to 15%. There was a further increase in the coarse, quartzose content to >20% following the damming of the Nile River (Aswan High Dam, in 1964), continuing the earlier post-LIA increase.

The geochemical data suggests a shift in the composition of the finer-grained sediments at the end of the LIA. During the LIA, clay-rich sediments were found to have lower levels of K_2O and higher levels of Ni compared to sediments post-LIA. These likely indicate a change in the source of sediments to the eastern Mediterranean shelf, shifting from a dominance of Nile-derived sediments and Nile Delta soils during the LIA, to more Saharan-derived, fine-grained dust and coarse-grained quartzose sands in the post-LIA period. The prevalence of Nile-derived sediments during the LIA suggests wetter conditions in coastal East Africa during that time period, as opposed to post-LIA.

The foraminiferal data also indicate a shift at the end of the LIA, mainly in group composition and abundance. A major increase in miliolid shell-type abundances after the LIA, aligns with a transition to warmer temperatures post-LIA. An additional increase is detected in species richness and abundance after the damming of the Nile River. However, this is superimposed on the ongoing increase since the LIA termination.

1. Introduction

Human activities since the Industrial Revolution have left their impact on marine systems (e.g., Crutzen, 2002; Galgani, 2015), strongly influencing characteristics of shelf seafloors. Attempts were made to objectively assess the relative contribution of natural processes and anthropogenic factors in shaping these changes (Dietl et al., 2015), however, in the absence of high-resolution well-dated records it is challenging to pinpoint the timing and extent of the controlling factors. Detailed, long-term records that precede known human interventions are vital for providing the framework for understanding the extent of human effect on current seafloors. In particular, shallow marine environments are sensitive to human activity due to their relative proximity to the coast. Thus, acquiring high-resolution records from marine shelves is critical for studying historic change and for quantifying the rates of change that seafloors undergo today.

The Levantine basin, the southeastern-most section of the Mediterranean Sea, has been subjected to widespread environmental changes during the last centuries (e.g., Rilov and Galil, 2009; Lionello et al., 2023). These include both natural and anthropogenic changes, for example, the pronounced cooling of the Little Ice Age (Incarbona et al., 2010; Cosentino et al., 2017), the construction of the Suez Canal in the 19th century (Golani, 1998; Katsanevakis et al., 2014), the damming of the Nile River in 1964 (Stanley, 1988; Nixon, 2003; Zviely et al., 2007), coastal development, the discharge of untreated industrial and human waste (Kress et al., 2004) and other human-driven activities. As a result,

* Corresponding author.
E-mail address: yael@gsi.gov.il (Y. Edelman-Furstenberg).

https://doi.org/10.1016/j.quascirev.2025.109185
Received 4 June 2024; Received in revised form 31 December 2024; Accepted 3 January 2025
Available online 6 January 2025

the eastern Mediterranean shelf has experienced significant changes in the composition of benthic micro- and macrofauna (e.g., Galil and Zenetos, 2002; Hyams-Kaphzan et al., 2008, 2009; Coll et al., 2010; Comay et al., 2015; Leshno et al., 2015; Avnaim-Katav et al., 2020), in sediment characteristics (Sandler and Herut, 2000; Zviely et al., 2007; Katz and Crouvi, 2018) and in chemical composition of its seafloor (e.g., Bookman et al., 2021). Therefore, the eastern Mediterranean shelf is ideally positioned to act as a sensitive recorder of recent change. Furthermore, the proximity of the eastern Mediterranean coast to the discharge of Nile River sediments resulted in exceptionally high sedimentation rates during the early Holocene (Schilman et al., 2001; Avnaim-Katav et al., 2019; Bookman et al., 2021). The high sedimentation was associated with both regional and global climatic fluctuations, namely, the monsoonal climate system and ITCZ (Intertropical Convergence Zone) (e.g., Almogi-Labin et al., 2009; Box et al., 2011; Hennekam et al., 2014; Avnaim-Katav et al., 2019; Bookman et al., 2021). These high sedimentation rates enable to study the record of the late Pleistocene and Holocene in high resolution. However, information on the past ~250 years of globally-growing human influence is rare and data relevant to understanding the cause-effect relationship of human activity in the region are scarce due to limited high-resolution dated sedimentary records.

The goal of this study was to track major natural and human-driven changes recorded in the eastern Mediterranean by investigating a high-resolution well-dated sediment core from the Israeli shelf at ~60 m water depth. In particular, the focus was on the controlling factors governing the sediment composition of the area and on how they relate to known, recent, historic events. Detailed sampling and sediment dating, particle size distribution (PSD), microfossils (benthic foraminifera), mineralogical and geochemical analyses (major and trace elements, total organic carbon) were combined to better understand the rate and extent of human activity in shaping current seafloor patterns, and especially the past ~250 years of anthropogenic influence in the eastern Mediterranean.

1.1. Eastern Mediterranean Israeli shelf

The Levantine basin in the eastern Mediterranean is land-locked and is strongly affected by fresh water and sediment input from the Nile River. Sediments are primarily distributed eastward across the Nile Delta and then northward as far as northern Israel (Stanley, 1988, 1989) and farther. They are transported along the inner shelf by longshore, anticlockwise currents, while wind-induced currents transport the sediments deeper into the sea (Rosentraub and Brenner, 2007; Schattner, 2021). The 180 km long Israeli coastline, trending N-NE to S-SW, is part of the eastern border of the Levantine basin (Por, 1989), the easternmost section of the Mediterranean Sea. The shelf narrows from 25 to 30 km in the south to less than 10 km in the north (Rosentraub and Brenner, 2007), with bathymetric contours aligned sub-parallel to the coastline. The upper 120 m of the Levantine water column is stratified during most of the year but becomes homogenous during winter when surface cooling causes deepening of the mixed layer (Herut et al., 2000; Rosentraub and Brenner, 2007).

The Nile River is one of the most important rivers flowing into the Levantine basin. The construction of the Aswan High Dam in 1964 significantly decreased the input of nutrients and sediments into the Mediterranean (Stanley, 1988; Halim et al., 1995; Krom et al., 1999; Herut et al., 2023). This decline was superimposed on the already extreme environmental conditions characterizing the Levant Basin: oligotrophy, high salinity and high surface-water temperatures (Por, 1989; Herut et al., 2000, 2023; Coll et al., 2010). The majority of shelf sediments post-Aswan Dam are siliciclastics originating from the erosion of the Nile River delta, with a lesser contribution from local sources (Nir, 1984; Zviely et al., 2007). The dominant northern flow of surface water (Zviely et al., 2007) created a south-north gradient of seafloor substrates, with Nilotic siliciclastic sediments abundant in the south and decreasing northwards, where biogenic, carbonate-rich sediments are dominant (Hyams-Kaphzan et al., 2008). An east-west bathymetric gradient of grain size is characterized by sand dominating in shallow waters (up to ~35 m water depth) and silt and clay in deeper waters (Nir, 1984; Almagor et al., 2000; Almogi-Labin et al., 2012).

1.2. The Little Ice ge

The Little Ice Age (LIA) is mostly a North Atlantic phenomenon, but not only (Matthews and Briffa, 2005). It started ~1350 and terminated around 1850 and was characterized by low summer temperatures combined with high winter precipitation, and a general advancement of mountain glaciers (e.g., Grove, 2001; Büntgen et al., 2005; Matthews and Briffa, 2005), with the coldest interval from ~1550 to 1750 CE (Bradley and Jonest, 1993). On land, the temperature drop resulted in damaged crops and restriction of the vegetation period (Glaser and Riemann, 2009 and references therein).

A shift to cold ocean conditions at the onset of the LIA probably resulted in an increase in the cold, low-salinity polar waters in the north Atlantic (Moffa-Sánchez et al., 2014). This LIA cooling is also observed in calcareous nannoplankton and benthic foraminiferal assemblages from the Mediterranean and north Atlantic (e.g., Incarbona et al., 2010; Perner et al., 2013).

2. Materials and methods

This study focused on a representative site at 60 m water depth in the central Israeli shelf, off the coast of Herzelia (Fig. 1a). The site comprises a soft-bottom seafloor within the silty sediment seafloor zone (Almogi-Labin et al., 2012) and is positioned in waters deeper than any known range of major pollution, especially far from coastal anthropogenic influence (Kress et al., 2004; Pasternak et al., 2019). A long gravity core (190 cm) that penetrated deep enough to capture ^{210}Pb background levels was retrieved (R/V Bat Galim cruise during summer 2018) in order to estimate sedimentation rates. Upon retrieval on deck, care was taken to keep the core vertical as to not disturb the top sediment.

The core (diameter 6.4 cm) was sliced into 1 cm increments down to 84 cm and used for analysis of ^{210}Pb activity (dating), sediment granulometry, sediment chemistry, mineralogy, percent total organic carbon (TOC) and microfossil (foraminifera) abundance.

2.1. Sampling and analytical methods

2.1.1. ^{210}Pb sediment processing

Age determination was done using ^{210}Pb on the fine fraction of the sediment (<63 μm), which due to its larger specific surface area is richer in adsorbed excess ^{210}Pb than the coarse sediment fraction. This approach has recently proven to be successful in dating sediments with low ^{210}Pb activity (Edelman-Furstenberg et al., 2020).

A total of 36 sediment slices were weighed and then lyophilized for the water content of the sediment. Approximately 25 g from each increment was then wet-sieved with Milli-Q water (>17 MOhm/cm) over a 63 μm sieve, left to settle for 14 days, and then the excess water decanted. The remaining wet sediment was oven-dried at 50 °C to determine the wt-% fines <63 μm. Part of the fine fraction was sent to the Royal Netherlands Institute for Sea Research (NIOZ) for ^{210}Pb analysis and determination of sedimentation rate, focusing on every other cm down to 60 cm and then every 3rd and 6th down to 84 cm. This was done to make sure of reaching supported ^{210}Pb levels in the core.

2.1.2. Alpha spectrometry of ^{210}Pb

Due to the arid environment and limited precipitation and river runoff into the Israeli Mediterranean, we chose to determine ^{210}Pb through alpha spectrometry measurement of its granddaughter isotope ^{210}Po after chemical extraction from the sediment matrix. Alpha spectrometry counting is significantly more accurate and sensitive compared

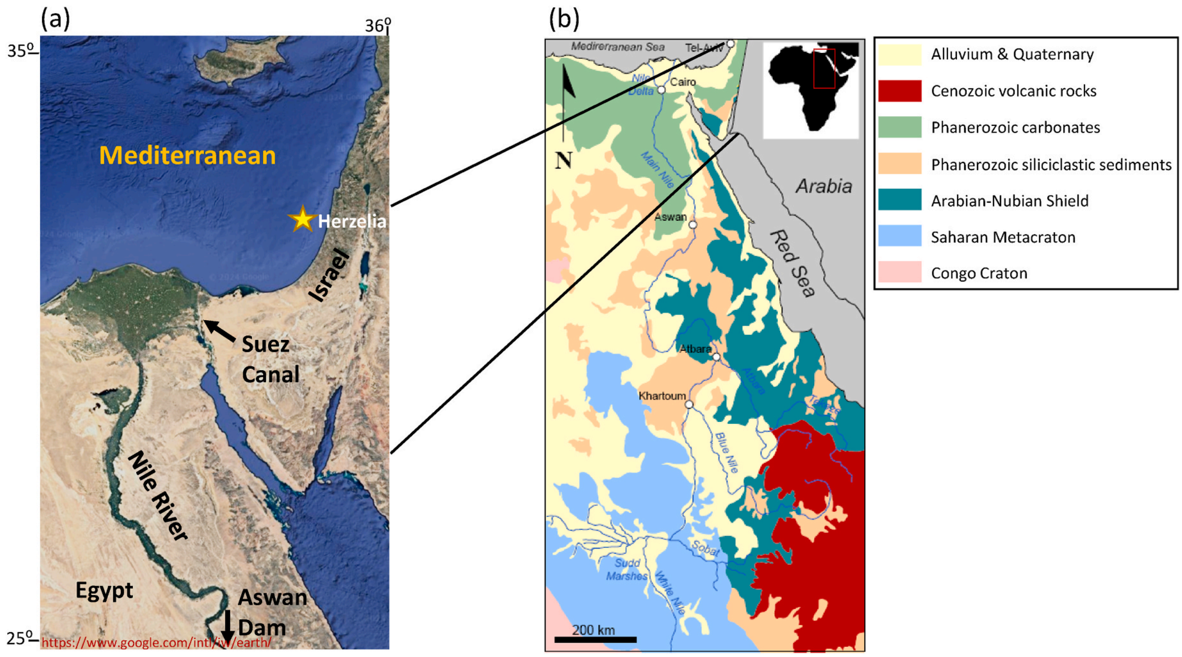

Fig. 1. (a) Study area and core site (marked by a star) in 57 m water depth, off the coast of Herzelia, Israel. (b) Simplified geological map of the Nile drainage area (modified after Fielding et al., 2018).

to gamma-ray spectrometry (e.g., Baskaran, 2011), and was used in other eastern Mediterranean locations for determining sediment accumulation rates in surface sediment cores (Bareket et al., 2016; Ashkenazi et al., 2022; Herut et al., 2023; Moshe et al., 2024). Lab procedures follow those of Edelman-Furstenberg et al. (2020).

2.1.3. Particle size distribution (PSD) analysis

Grain size analysis was conducted in 2 cm intervals down to 84 cm (total of 41 samples) using Malvern MS-2000 laser diffraction over the particle-size range of 0.02–2000 μm. The measurement procedure included dispersion (using sodium hexametaphosphate solution), stirring for 5 min, and ultrasonication for 30 s. Three to six replicate specimens of each sample were then subjected to three consecutive 5 s runs at a pump speed of 1800 RPM. The laser diffraction raw values were transformed into PSD using the Mie scattering model, with optical parameters of $RI = 1.52$ and $A = 0.1$.

2.1.4. Bulk mineralogy

Forty three samples were spiked with 20% (wt.) corundum, milled using a ball-mill and side-loaded into aluminum holders. XRD patterns were acquired in Bragg-Brentano geometry using a PANalytical X'Pert diffractometer with CuKα radiation operated at 45 kV and 40 mA. The samples were scanned from 9 to 70° 2θ at a step size of 0.013° 2θ, using a PIXcel detector in continuous scanning line (1D) mode with an active length of 3.35°. Mineral phase identification was done using HighScore Plus® software based on ICSD database. Semi-quantitative phase abundances were estimated using the normalized (peak area) relative intensity ratio (RIR) method (e.g. Jenkins and Snyder, 1996), using in-house RIR values measured on the same instrument under similar settings.

2.1.5. Clay fraction mineralogy

The clay fraction from 43 samples (<2 μm) was collected from suspensions settled according to Stokes Law after: 1) carbonate minerals and salts dissolution by buffered acetic acid; 2) saturation in $SrCl_2$ (0.03 M); and 3) disaggregation by a low-intensity ultrasonic treatment for a few minutes. Clay suspensions were pipetted onto glass slides and analyzed after air-drying, glycolation (at least 8 h at 60 °C), and heating for 2 h to 550 °C (Moore and Reynolds Jr, 1989). Samples were scanned from 2 to 30° 2θ with a step size of 0.013° 2θ using the detector in continuous scanning line (1D) mode with an active length of 1.01°. Semi-quantitative clay abundances were estimated from the relative peak areas of I-S, kaolinite, illite and chlorite following the method of Biscaye (1965).

2.1.6. Chemical analysis

Whole sediments (47 samples) were used for the determination of the chemical composition, while the <150 μm fraction (42 samples) was used in order to enrich the amount of trace elements and total organic carbon (TOC) in the samples. All samples were crushed using a ball mill (Pulverisette 2, FRITSCH, Germany). Powdered samples were fully dissolved by fusion with lithium metaborate ($LiBO_4$) for major elements and with sodium peroxide (Na_2O_2) for trace elements (Brenner et al., 1980; Yu et al., 2001). Major elements were measured by Inductively Coupled Plasma Optical Emission Spectrometry (ICP-OES; Optima 5300, PerkinElmer, USA), and trace elements by Inductively Coupled Plasma Mass Spectrometry (ICP-MS; Nexion 300D, PerkinElmer, USA). Calibration was performed using commercial elemental solutions. Various certified reference materials (CRMs) were processed and analyzed along with the samples for quality control of the major composition (BCR-32, BCS-393, BCS-313, JB-1, SCO-1, SO-3, RGM-1, 1633A, and JP-1) and trace elements (JB-1, SCO-1, SO-3, and 1633A) analyses. Loss on ignition (LOI) was performed by 1050 °C combustion for 4 h and the weight loss was recorded. The TOC analysis was determined by potentiometric titration (Gelman et al., 2012).

2.1.7. Benthic Foraminifera analysis

Foraminiferal analysis was performed on every 2–3 cm down to 84 cm (34 samples in total). Bulk samples were dry weighed, washed over a 63 μm sieve, and foraminifera shells larger than 150 μm were dry-picked and analyzed using a stereomicroscope. Large samples were randomly split into sub-samples containing ~250–300 specimens. The foraminiferal tests were investigated as sediment particles in order to correlate between variations in the grain size and foraminiferal numerical abundances per gram dry sediment. The proportions of the three main shell-type groups: perforate calcareous, miliolid and agglutinated, were calculated down the core as well as the number of species per sample. Statistical analyses were performed using GraphPad Prism 7 software. Analysis of variance (one-way ANOVA) followed by Bonferroni's multiple comparisons tests were performed on foraminiferal abundance and species diversity to identify the differences between groups.

3. Results

3.1. ^{210}Pb depth profile and model fit

The top layer of the core is of brown sediment that changed to grey below a depth of 21 cm, and becoming finer-grained at the bottom of the core (Fig. 2). Water content did not show strong shifts, however percentages were slightly lower in the top 30 cm increasing downcore, with highest percentages deeper than 60 cm.

The profile of ^{210}Pb is continuous, lacking an evident surface mixed layer. The depth profile yielded activities of ^{210}Pb ranging from 126 in the top sample to ~10 mBq g^{-1} at the bottom of the core. The depth profile with the best fit was a CFCS model without a surface mixed layer (Fig. 2). Accordingly, the biological mixing coefficient was taken as negligible (D_b = 0.0001 cm^2 y^{-1}). The ^{210}Pb activity is given in Supplementary Table S1.

Extrapolating the modelled average sediment accumulation rate for the fine fraction, of 0.32 cm y^{-1}, the bottom of the core dates to the year 1750. The core thus represents a time interval extending beyond the full duration of the Anthropocene (Zalasiewicz et al., 2021). By interpolation, the termination of the Little Ice Age (LIA) as suggested for Europe, in 1850, is located 55 cm downcore, whereas the construction of the Aswan High Dam on the Nile River during the mid-1960 is located at 17 cm down the core. The sedimentation rate found by fitting the CFCS model (widely used in marine settings) represents an average over the approximate 150 years where excess ^{210}Pb is present, thus, the derived dates are only approximate.

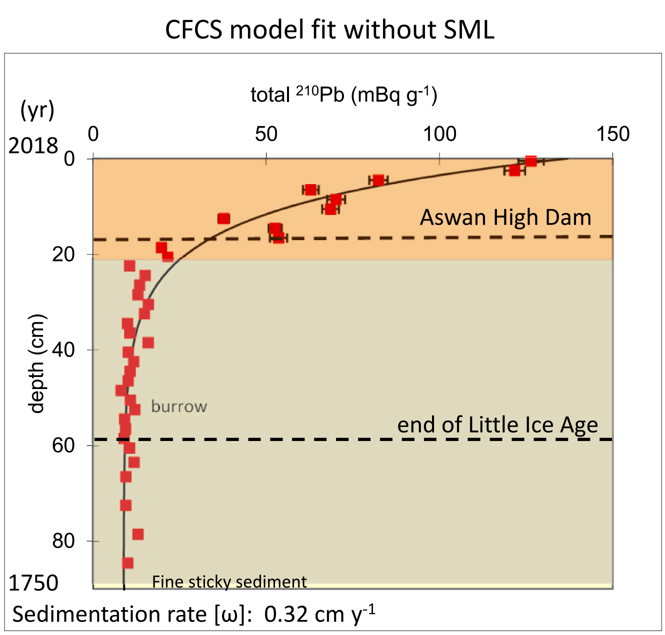

Fig. 2. Depth profile of total ^{210}Pb activity measured in the fine fraction of the studied sediment core retrieved from 57 m water depth. The exponential curve over the data represents a constant flux constant sedimentation (CFCS) model without surface mixed layer (SML), fitted to determine average sedimentation rate. The top, brown sediment was coarser than the grey, finer sediment at the bottom of the core. (For interpretation of the references to colour in this figure legend, the reader is referred to the Web version of this article.)

3.2. Particle size distribution

All PSDs are bi-modal, with a fine mode in ~5 μm (clay to fine silt) and a coarse mode in 50–60 μm (coarse silt) (Fig. 3a). The two modes are separated by a minimum located at 15–20 μm. The amplitude of these modes changes along the core and with time – in the lower parts of the core the fine mode is the dominant one, while the coarse mode becomes more and more dominant up the core, towards the 20th century. This coarsening trend with time is emphasized when plotting (1) a ratio between these two modes (the percent of >20 μm divided by the percent of <20 μm, termed the 20 μm ratio, see Crouvi et al., 2008) and (2) the percent of the sand fraction, along the core (Fig. 3b). The finest-grained sediment, composed of 95% or more of silt and clay and only 5% or less of sand, was deposited during the LIA. After the LIA and until the mid 1960's distinctly coarser sediment was deposited (7–15% sand). After the mid 1960's a further coarsening is observed, with sand content increasing to more than 20%.

3.3. Mineralogy

The complete mineralogical data is given in Supplementary Table S2. The bulk mineralogical composition of all samples includes phyllosilicates as a dominant component. However, a clear trend of decreasing phyllosilicates can be seen throughout most of the core, from a relatively stable average value of ca. 75% in the samples deeper than 60 cm (LIA period) to ca. 55% in the shallowest samples (Fig. 4a). Quartz and calcite show an enrichment trend of from 6 to 3.5%, to 15.5 and 7.5%, respectively (Fig. 4b and c). In particular, the quartz component shows a significant increase from ~6 to ~11% within the depth interval of 60 to 50 cm, followed by relative stability between 50 and 20 cm depth and then steady increase from ~11 to ~15.5% in the upper 20 cm of the core (Fig. 4b). An intriguing trend is seen in the ratio of the feldspar minerals (Fig. 4d). Below 60 cm depth the plagioclase/K-feldspar ratio is highly variable with extreme values reaching 9–11, whereas above this depth the plagioclase/K-feldspar ratio is relatively constant, at a value of ~1. The decrease of phyllosilicates and the increase in quartz and calcite up the core is consistent with the increasing grain sizes (Fig. 3b).

3.4. Geochemistry

The complete geochemical data is given in Supplementary Table S3. Selected element trends throughout the studied core are presented in Fig. 5. Silica (SiO_2) content shows a continuous increase from near constant values of ca. 47 wt% below 60 cm depth – the end of the LIA, to ca. 52 wt% in the shallowest samples. Calcium (CaO) content indicates a similar trend of enrichment although this enrichment trend seems to start from 1800 and not from the end of the LIA. Alumina (Al_2O_3) and iron (Fe_2O_3) contents display an opposite trend of depletion, from relatively stable values of ca. 16 and 11 wt%, respectively, at the end of the LIA, to ca. 13 and 9 wt%, respectively, in the surface samples. These two elements also show a strong correlation of R^2 = 0.95 (Fig. 6a). Potassium (K_2O) displays a conspicuous increase at the end of the LIA from values of 1.4–1.5 wt%, to slightly, but distinctly, higher values of 1.6–1.8 wt% that persist to the top of the core (Fig. 5e and 6b). The depletion in Al_2O_3 up the core is consistent with the decrease of phyllosilicates, and the enrichment in SiO_2 and CaO is consistent with the increase in quartz and calcite (Fig. 5a–d). The low K_2O concentrations in the samples below 60 m, dated to the LIA, is consistent with their low K-feldspar content (Fig. 5e). Most of the studied trace elements show a general trend of depletion upcore, along with the trends in Al_2O_3 and Fe_2O_3 (e.g., Cu, Nd, Ni and Co; Fig. 5f–i).

The total organic carbon (TOC) content displays a general depletion throughout the studied core, from 0.6 to 0.8 in the lower part to 0.2–0.4 wt % up the core. However, this trend can also be divided into a relatively stable stage of higher TOC content during the LIA (below ca. 60 cm), followed by a stage of depletion in TOC towards the present that is

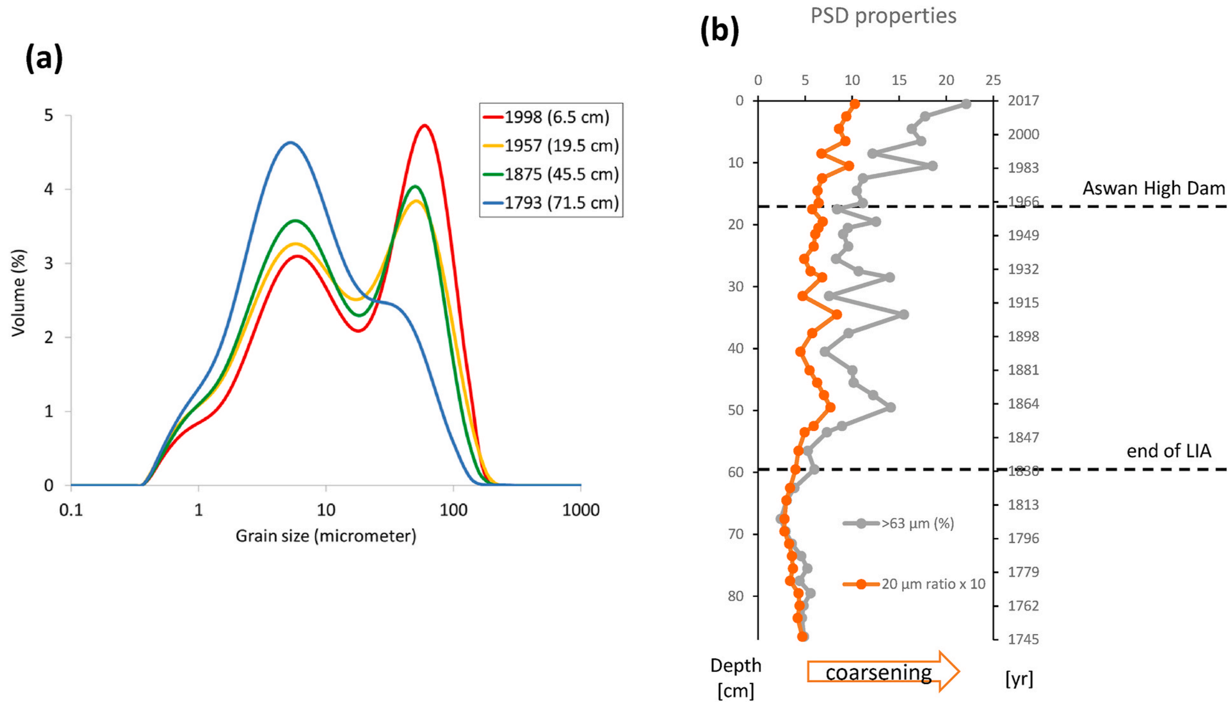

Fig. 3. (a) Particle size distribution graphs, showing bi-modal distribution, and (b) the percent of the sand fraction and the 20 μm ratio along the core. See text for further explanation.

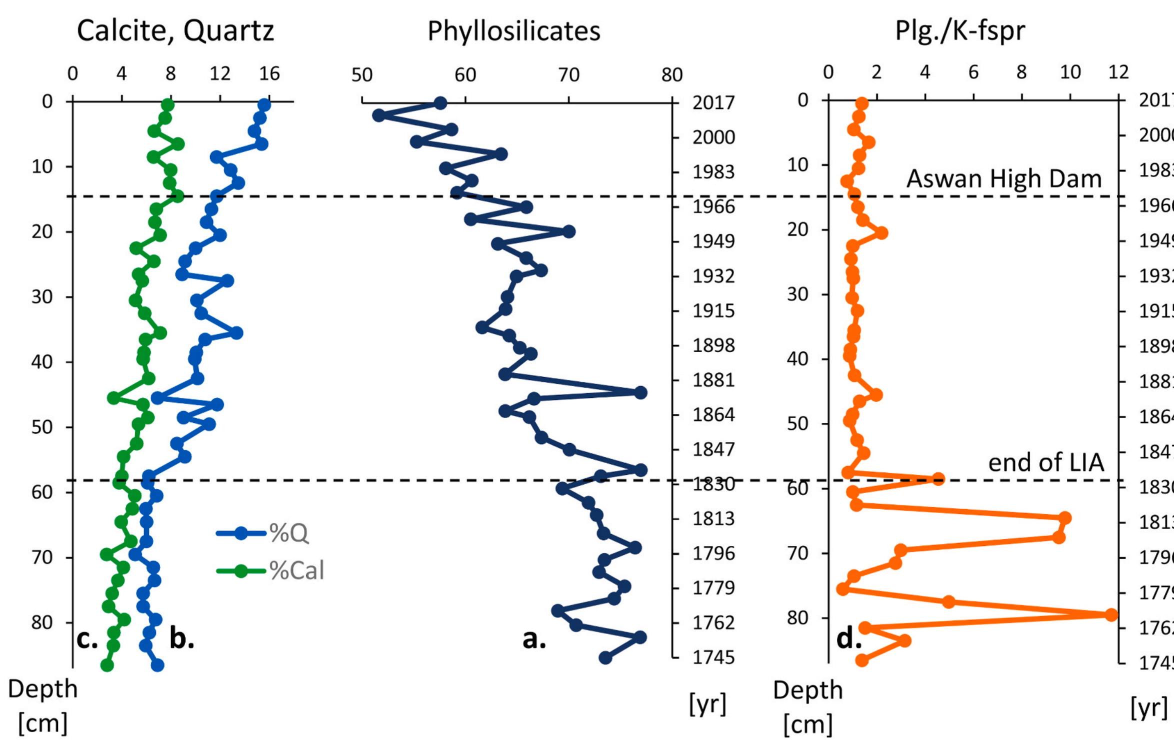

Fig. 4. Down-core profiles showing the concentrations of selected minerals. Dashed lines mark the approximate end of the Little Ice Age (1830 CE) and construction of the Aswan High Dam on the Nile River (1964 CE).

especially pronounced after the damming of the Nile River by the Aswan High Dam (Fig. 5j).

3.5. Distribution patterns of benthic foraminifera

The dead foraminiferal assemblages (>150 μm) demonstrate remarkable differences in their numerical abundances downcore (Fig. 7; Supplementary Tables S4a and b). In general, the numerical abundance shows high fluctuations and increases to values of >200 individuals per gram dry sediment in the top 17 cm (post Aswan High Dam). Medium abundances of 50–100 were detected in the post-LIA samples, and fewer fluctuations and very low abundances of 25–50 in the deepest part of the

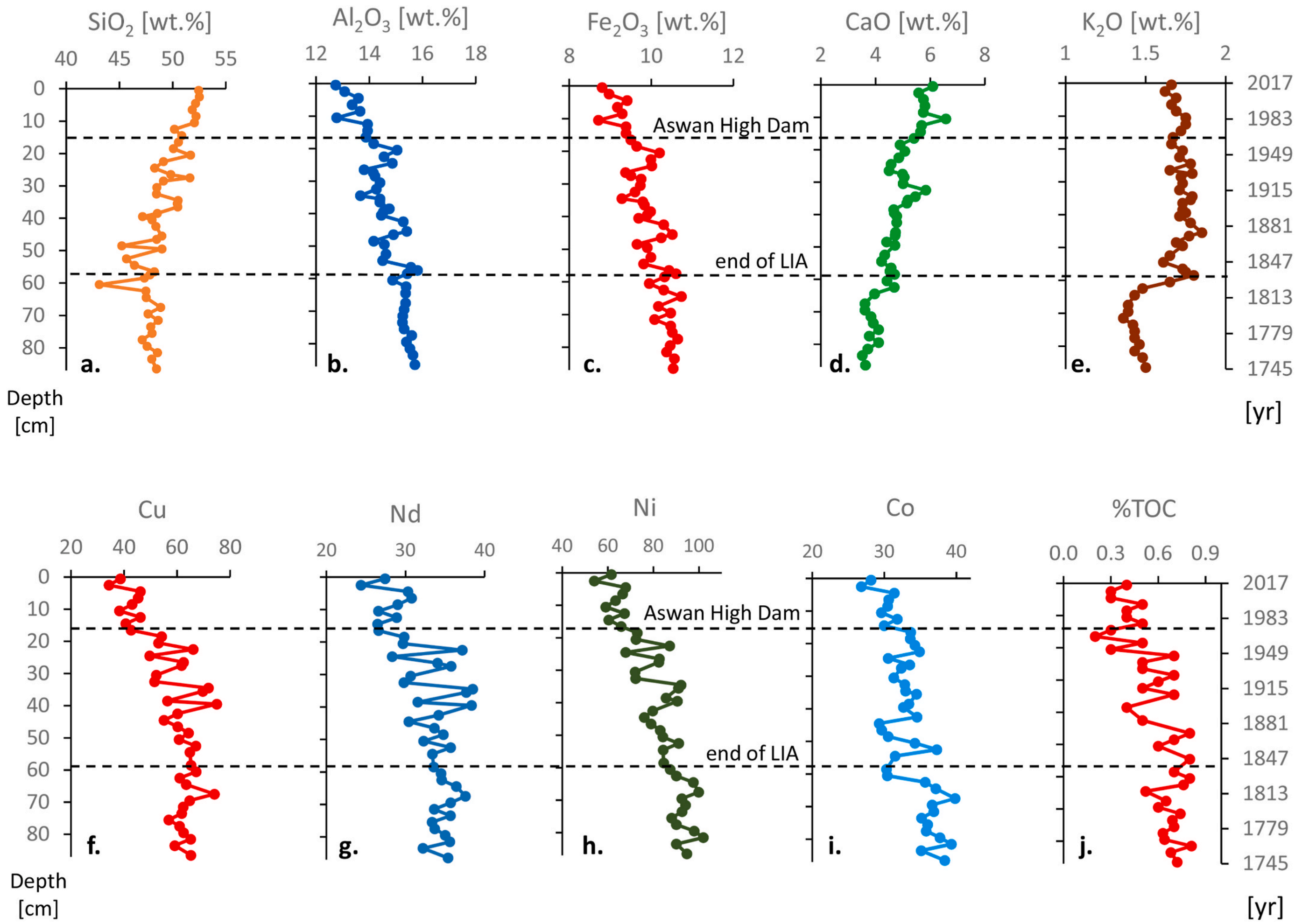

Fig. 5. Down-core profiles showing the concentrations of selected major oxides, trace elements and total organic carbon (TOC). Dashed lines mark the approximated end of the Little Ice Age (1830 CE) and construction of the Aswan High Dam on the Nile River (1964 CE).

core (LIA) (Fig. 7). LIA species richness showed minimum values of 35-19 at the bottom of the core. Between 60 and 17 cm (post-LIA samples), diversity increases, ranging between 39 and 57 species. The highest species number was detected in the upper 17 cm of the core (post-Aswan High Dam), with 60–80 species per sample. A one-way ANOVA shows significant variation in the foraminiferal numerical abundance [$F(2,31) = 35.67$, $p < P < 0.0001$] and species richness [$F(2, 31) = 55.19$, $P < 0.0001$], and post hoc Bonferroni detected significant differences between all three time-intervals (Aswan High Dam, post-LIA and LIA).

The majority of the foraminiferal assemblages are composed of perforate-calcareous species reaching a maximum of 80% (Fig. 8). The ratio between the relative abundances of perforate-calcareous and miliolid species is 4:1 at the end of the LIA decreasing to 2:1 afterwards (Fig. 8). The miliolid shell-type group abundance increases to ~40% at the post-LIA time period. Along with this increase in relative abundance of the group an increase in miliolid species was observed. In the LIA and post-LIA miliolids reached a maximum of 26 species, while at the top 18 cm of the core the miliolids comprise 47 species, (Supplementary Table S4b).

4. Discussion

4.1. Sediment accumulation rates in the continental shelf of the eastern Mediterranean

The sedimentation regime and rate of accumulation for the Israeli slope and basin are generally known for most of the Holocene (e.g., Krom et al., 1999; Schilman et al., 2001; Box et al., 2011; Hennekam et al., 2014; Hennekam, 2015 and refs therein), yet the recent past (i.e., the last couple of centuries), characterized by increasing human activity, is less studied.

Holocene sediment accumulation rates reported for the Israeli shelf, based on ^{14}C dating, range from ~60 to 420 cm/kyr (Tapiero, 2002; Avnaim-Katav et al., 2019; Agiadi and Albano, 2020). For surface sediments dated by means of ^{210}Pb, rates range from 50 to ~200 cm/kyr (Bareket et al., 2016; Herut et al., 2023). At 40 m water depth off Herzelia, Almogi-Labin and other (2009) and Kalman and others (2022) mentioned ~200 cm/kyr.

The present studied core from 60 m water depth, penetrated the sediment deep enough to capture background levels of ^{210}Pb at ~40 cm core-depth (Fig. 2). This allows us to improve the rates extrapolated from other short cores taken in the Israeli Mediterranean shelf, which were too shallow to detect the supported ^{210}Pb levels (e.g., Bareket et al., 2016). Our study records an average sedimentation rate of 320 cm/kyr for sediments from ~60 m water depth, thus allowing for the first time, a high-resolution examination of the last ~270 years in the southeastern Mediterranean.

4.2. Bioturbation regime at 60 m water depth

The eastern Mediterranean is known for its oligotrophic waters and seafloor depleted in organic carbon (see review in de Madron et al.,

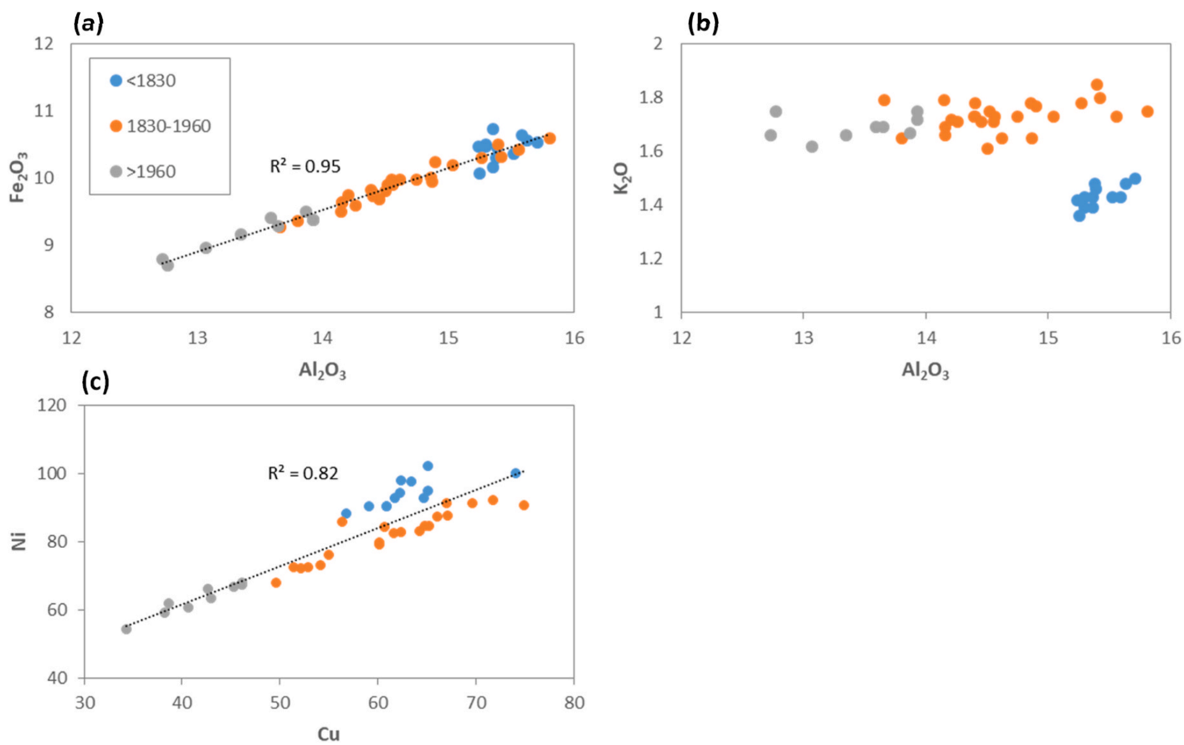

Fig. 6. Correlation diagrams between selected major oxides (in wt.%) and trace elements (in ppm) in the studied samples grouped by age. The correlation coefficients (R^2) include all core samples as one group.

2011) that greatly limits the activity of the dominating burrowing fauna on the seafloor. Biological activity on the seafloor naturally produces a mixed surface layer, mixing the sediment to the depth of infaunal activity. However, deep burrowing fauna is relatively scarce on organic carbon depleted seafloors, thus overall, limiting bioturbation and sediment mixing of the seafloor.

Our samples exhibited extremely high abundances of the brittle star *Ophiura ophiura* (covering between 20 and 60% of the surface area of the core-sediment). This brittle star has a continuous distribution from the North Sea to the eastern Mediterranean and is the main species in the Israeli Mediterranean (Fishelson, 2000). *O. ophiura* is usually found in shallow waters, with a preference for soft sediments (Boos et al., 2010). It is a hunter-scavenger that rather than burrowing, shows a fleeing mechanism from other predators as an escape mechanism (Hill and Tyler-Walters, 2018 and references therein). Furthermore, no significant bioturbation of seafloor sediments is attributed to this species.

It seems that the oligotrophic nature of the eastern Mediterranean together with the high abundances of brittle stars covering the surface of the seafloor at 60 m resulted in minor bioturbation of the seafloor at this water depth. Furthermore, the relatively high sedimentation rate recorded for the eastern Mediterranean also acts to mask the effects of bioturbation. Consequently, the sediment at the Herzelia station was relatively undisturbed by bioturbation.

4.3. Sediment provenance

The amount of sand attained in the surface sediment of the core (16–22%) is comparable to that previously reported by Almogi-Labin and others (2012) for their 60-m water depth station off Herzelia (16%), sampled in 2009. Past studies showed a coarsening of grain size in surface sediments, which was suggested to be associated with the termination of the sediment flow from the Nile River after the construction of the Aswan High Dam in 1964 (e.g., Almogi-Labin et al., 2012; Bookman et al., 2021; Kalman et al., 2022; Herut et al., 2023). However, as shown in our results, this coarsening started well before the Aswan Dam construction and can thus not exclusively be attributed to human influence. Rather, we suggest a change in the climatic regime as a probable cause for the sediment change detected after 1830.

The grain size, mineralogical and geochemical results all indicate the existence of two major sedimentary components comprising the sediments at 60 m water depth: (1) a fine-grained, ferro-aluminous component with higher phyllosilicate content, dominant in the lower part of the core, and (2) a coarse-grained component with high quartz, calcite and feldspar content, becoming more abundant in the upper part of the core. Principle Component Analysis (PCA) of the normalized geochemical and mineralogical data from the sampled core (Fig. 9) shows the samples cluster along depth, with a clear separation of the three time intervals; LIA, post LIA before the construction of the Aswan High Dam, and the years after the Aswan Dam. Due to their distinct grain size, variations between the two components in the sediment can reflect variations in local energetic conditions at the depositional site. However, because the studied section was deposited under water depth of about 60 m, well below the wave baseline (Hyams-Kaphzan et al., 2008), local depositional effects seem unlikely. Hence, the relative shift from fine-grained phyllosilicate dominance in the lower part of the core to coarse-grained quartzose component in its upper part reflect a change of sediment provenance in this region of the Mediterranean. The fine-grained aluminosilicate-dominated sediment at the lower part of the core is consistent with sediments derived from Ethiopian flood basalts and Nubian shield basement rocks within the Blue Nile catchment, wheras the coarse quartzose sediment is consistent with sands derived from the Saharan dune fields (Garzanti et al., 2018).

The remarkable correlation between Al_2O_3 and Fe_2O_3 (Fig. 6) indicates that Fe is either a major component of the fine-grained phyllosilicate minerals, mainly illite-smectite, or that fine-grained iron-oxides are favorably transported and precipitated together with the phyllosilicates due to their similar grain size. In either case, the Al_2O_3 – Fe_2O_3 correlation found in the studied eastern Mediterranean sediments, is similar to that observed in three sets of local soil samples; from the nearby continental Israel (Sandler, 2013), from the Sahara desert

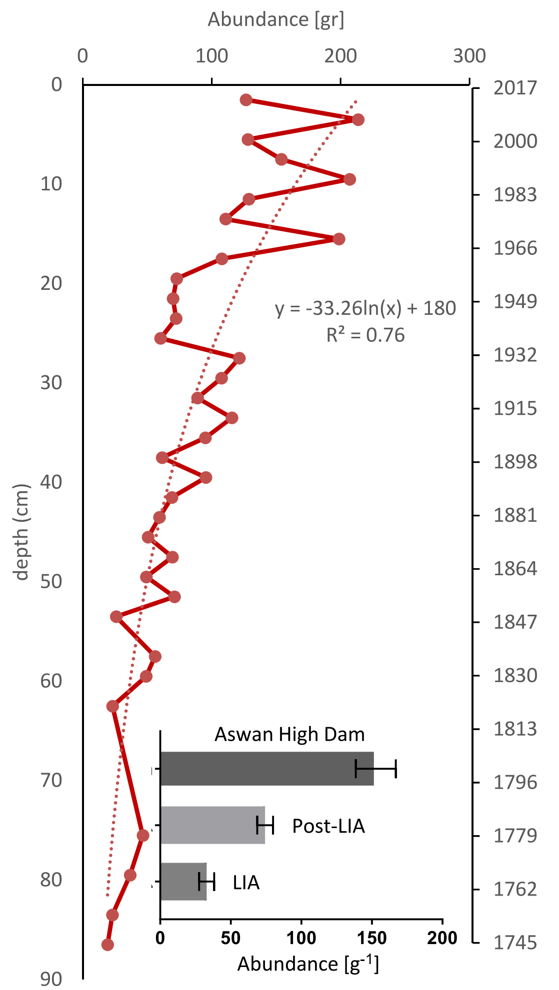

Fig. 7. Benthic foraminiferal numerical abundance per gram [gr] sediment along the studied core. A logarithmic curve (dotted line) was fitted to the data points. The equation of the fitted curve is shown on the right. Insert: The abundance data grouped by periods of Little Ice Age (LIA), post-LIA and Aswan High Dam samples. Bar graphs represent means ± STD.

(Moreno et al., 2006; Maryol and Lin, 2015) and from the Nile Delta (Abu Khatita, 2011). In contrast, fine-grained muds collected along the banks of the active Nile River and its tributaries do not show any Al_2O_3 – Fe_2O_3 correlation and extend to much higher Fe_2O_3 content (Garzanti et al., 2015) (Fig. 10a). This difference in chemical composition between local soils and Nile riverbank sediments may be explained by the process of chemical weathering in soils. Both Al and Fe are relatively stable elements and tend to concentrate in the solid fraction, as major constituents of the secondary minerals – phyllosilicates and Fe-oxides formed during pedogenic processes, thus, resulting in their mutual increase in soils and sediments derived from their weathering (e.g. Sandler et al., 2015). Sediments along the Atbara River, the Blue Nile and the main Nile banks are relatively freshly eroded, mostly from magmatic terranes of the Arabian-Nubian shield and the Ethiopian plateau basalts, which reside under strongly seasonal, semiarid climate (Garzanti et al., 2015). Therefore, these sediments comprise predominantly primary magmatic minerals, such as pyroxene, amphibole and feldspars, which have different and variable Fe/Al ratios. Accordingly, the Al_2O_3 – Fe_2O_3 correlation observed within the Mediterranean core sediments indicates the derivation of their fine-grained fraction from recycling of soils, by aeolian or local fluvial processes, rather than directly from Nile-transported sediment. However, the recycled soils may have developed on top of such Nilotic sediments within the Nile River delta, or completely outside of the Nilotic system. The apparent absence of

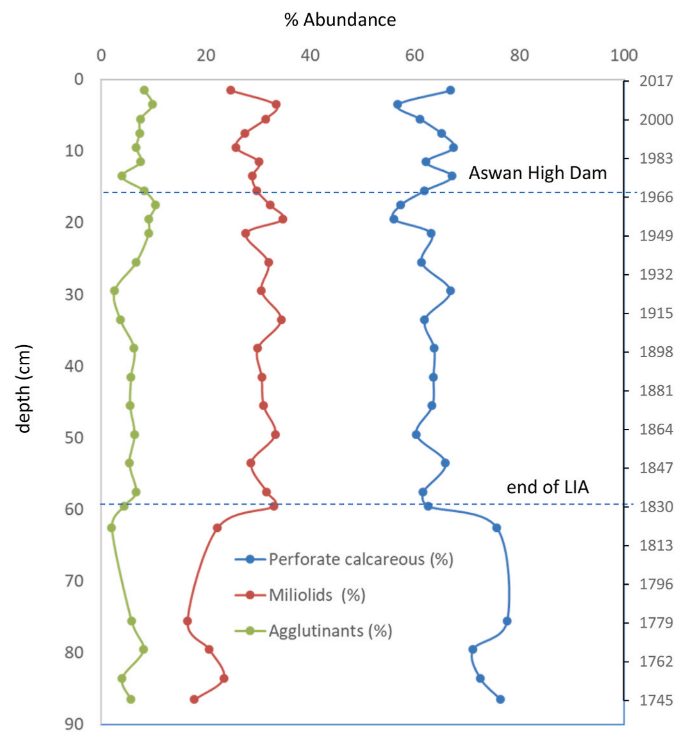

Fig. 8. Cumulative relative abundances of the three main foraminiferal groups along the core: perforate-calcareous, miliolids and agglutinated.

directly-transported Nile sediments in the studied core, according to the Al_2O_3 – Fe_2O_3 data, may be explained by the deposition of the coarser magmatic minerals in the Delta and near-shore invironment, preventing them from reaching the deeper basin, where finer clayey matrial often formed as secondary minerals in soils accumulates.

At the end of the LIA, a subtle yet distinct shift in K_2O concentration and trace element correlations is detected, indicating two separate fine-grained components, derived from different source terrains and/or under different weathering environments. During the LIA period, Al_2O_3 (clay)-rich samples have distinctly lower K_2O content and higher Ni/Cu ratio (Fig. 6b and c). A notable correlation is observed between Cu and Ni, in which the higher concentrations of Cu and Ni separate into two sub-parallel trends that correspond to sample depth (Fig. 6c). Samples deeper than 60 cm, dated to the LIA (prior to 1830), fall within the upper, higher Ni/Cu trend, whereas samples between 60 and 17 cm depth, dated to 1830–1960, fall within the lower Ni/Cu trend. The shallow samples, above 17 cm, dated to post construction of the Aswan High Dam in the mid-1960s, all plot at the low Cu and Ni end of the correlation line (Fig. 6c). The lower K_2O content in these samples is very similar to that measured in recent and buried soils of the Nile Delta (Abu Khatita, 2011), which is positioned along the higher Al_2O_3 and K_2O end of a common trend for all Nile riverbank mud samples (Garzanti et al., 2015). Younger, post-LIA samples have relatively higher K_2O content, similar to that measured in recent Saharan dust and soil samples (Moreno et al., 2006; Maryol and Lin, 2015) (Fig. 10b), probably arising from the abundance of K-feldspar in the Saharan basement rock (mostly Neoproterozoic metamorphic and granitic rocks, Abdelsalam et al., 2002) The Ni/Cu ratios in the LIA samples are also consistent with the Ni/Cu trend of the Nile riverbank mud samples (Garzanti et al., 2015), whereas younger post-LIA samples have lower Ni/Cu ratios, consistent with low Ni/Cu Saharan dust and soil samples (Moreno et al., 2006) (Fig. 10c). Higher Ni concentrations in the Nile-derived sediments are in accordance with the mantle source of the Ethiopian flood basalts covering vast area in the Blue Nile cathment area (Beccaluva et al., 2009).

Thus, it seems that the coarse quartzose component (sand) is

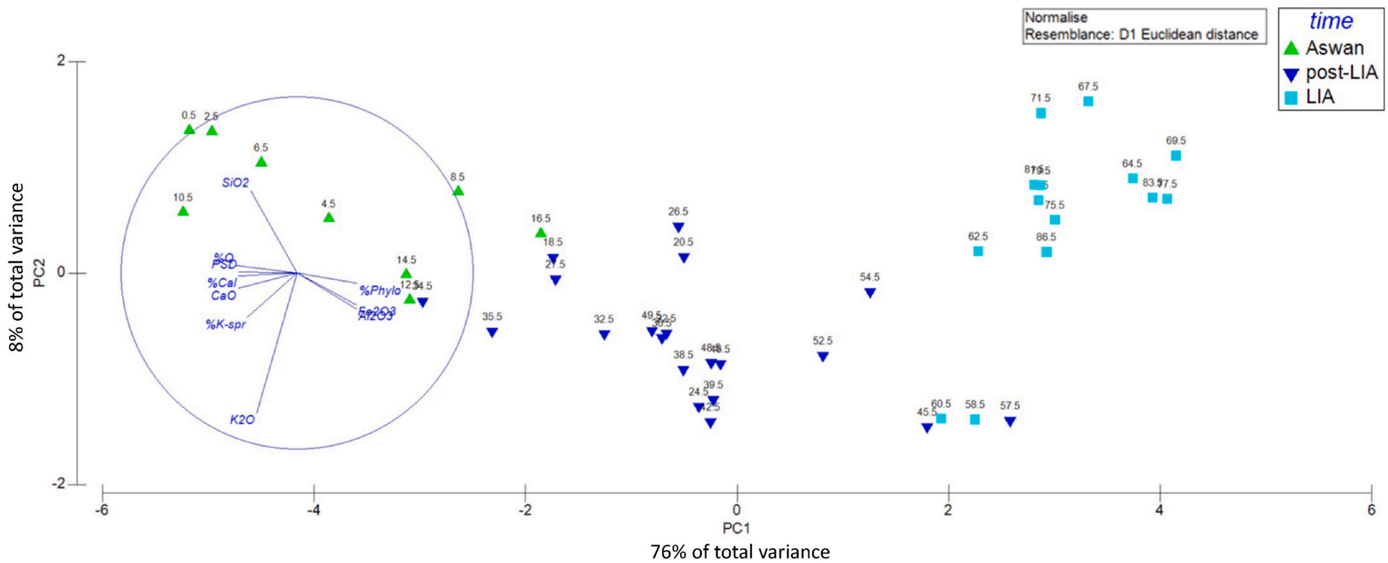

Fig. 9. Principle Component Analysis (PCA) of normalized geochemical and mineralogical data from the sampled core. The first axis describes 76% of the variance.

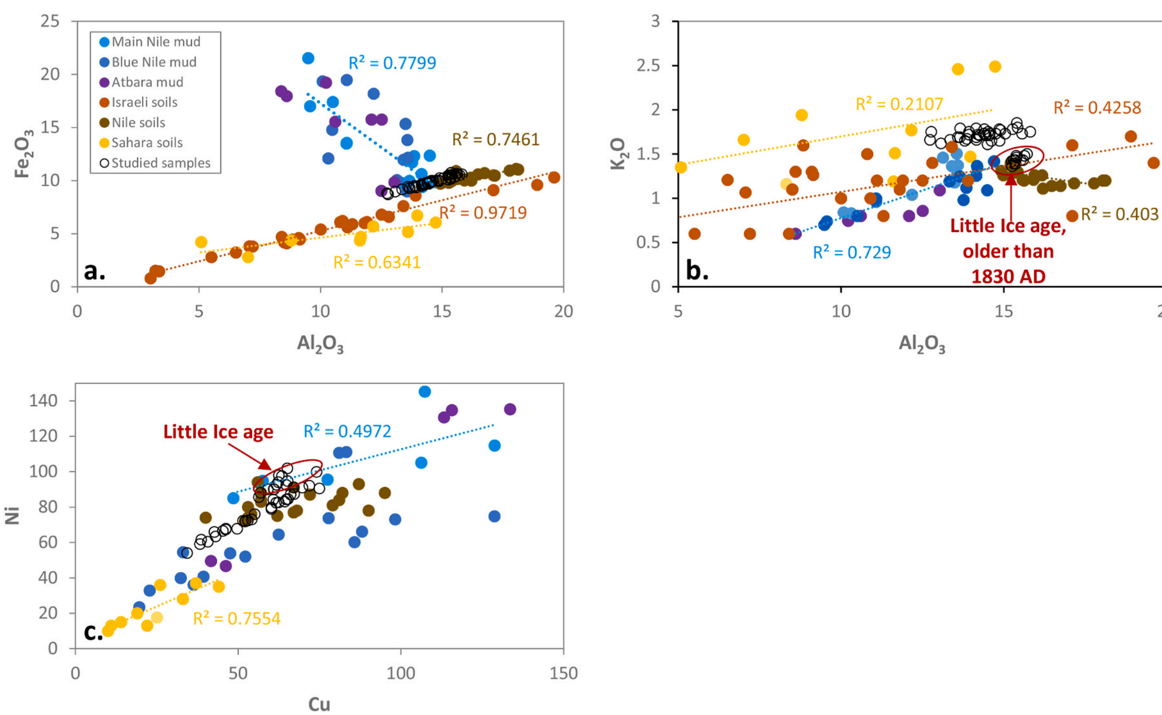

Fig. 10. Correlation diagrams between selected major oxides (in wt. %) and trace elements (in ppm) in the studied samples and other sediments of the region. Geochemical data for the Main Nile, Blue Nile and Atbara River bank sediments are from Garzanti et al. (2015) and references therein. Data for Israeli soils are from Sandler (2013). Data for Nile Delta soils are from Abu Khatita (2011). Data for Saharan soils and dust are from Moreno et al. (2006) and Maryol and Lin (2015). (For interpretation of the references to colour in this figure legend, the reader is referred to the Web version of this article.)

recycled by fluvial or aeolian processes from older siliciclastic sediments of North Africa, whereas the fine-grained, clayey component is derived from three different sources: Soils developed over Nilotic riverbank sediments, mostly within the Nile Delta area, Saharan desert soils probably transported by aeolian processes, and soils in the adjacent east Mediterranean region that were formed by mixture of dust from the two previous sources.

We suggest that during the LIA soils developed over Nilotic riverbanks were a dominant source for the Mediterranean sediments, based on their clayey composition that was relatively depleted in K_2O (and enriched in Ni/Cu). Following the termination of the LIA, it seems that the amount of fine-grained sediments derived from the Nile Delta soils diminished, leading to relative enrichment in the fine-grain component derived from other sources, most notably the Sahara desert. At the same time, there is a trend of relative enrichment in coarser-grained, quartzose and biogenic-calcitic (foraminifera) sediments (Fig. 6b, 7 and 10), which is also consistent with the relative decrease of fine-grain sediment input from the Nile system. This coarsening trend intensifies after the construction of the Aswan High Dam in the 1960s.

4.4. Temporal variation in benthic foraminifera distribution pattern

The foraminifera tests are part of the sedimentary particles >63 μm. Their abundance shows a similar upward increasing trend in the core as observed in the sand fraction (Fig. 3). The foraminiferal numerical abundance was higher post-LIA and highest after the construction of the Aswan High Dam (Fig. 7). This probably reflects the reduced dilution of foraminifera tests with fine sediments.

The continuous increase of the miliolid shell-type group from after the LIA and until the present (Fig. 8) may be associated with increasing temperatures after the termination of the LIA. Because the TOC content decreased only after the damming of the Nile (Fig. 5) it looks that oligotrophication alone does not affect the miliolid relative abundance. Moreover, field studies and laboratory experiments focusing on foraminiferal tolerance to modern thermal stress show that miliolids have a high tolerance to elevated temperatures (Murray, 1973; Arieli et al., 2011; Titelboim et al., 2016; Kenigsberg et al., 2022). Miliolids are also highly abundant and diverse (high species richness) in shallow waters along the Israeli coast between 40 and 60 m, with higher numbers during spring and summer when sea surface temperature increases (e.g., Hyams-Kaphzan et al., 2008, 2009; Avnaim-Katav et al., 2021). Our results in the eastern Mediterranean support this and show an increase in miliolid abundance together with the increase in temperature associated with the termination of the LIA (e.g., Bradley and Jonest, 1993). The trend of coarsening grain-size (and consequent oligotrophication) is superimposed on the ongoing trend that started after the LIA. The longterm historical data, conducted in the region for the first time, shows that the termination of the LIA, rather than the damming of the Nile River alone as proposed by others (e.g., Almogi-Labin et al., 2012; Bookman et al., 2021; Herut et al., 2023), is what had the most influence on the dominating foraminifera shell-groups (Fig. 8).

4.5. Recent climatic and sedimentological variations

One major event that is not well documented for Africa is the termination of the Little Ice Age. Our dated core and data identified this event, to occur in between 1830 and 1840, similar to 1850 as suggested for the termination of the LIA climate in Europe (e.g., Grove, 2001; Matthews and Briffa, 2005 and references therein).

Our record can be divided in two major periods (1) from ~1750 up to the termination of the Little Ice Age at ~1830, and (2) post LIA until the present, including the damming of the Nile River in the mid-1960s, which seemed to amplify the post-LIA trends (Fig. 11).

The period between the termination of the LIA and the industrial revolution is characterized by small fluctuations in the minerological, geochemical parameters and in foraminiferal abundances. It is characterized by finest grain sizes, clayey material, and increased levels of total organic matter, Ni and Cu (Figs. 3–5, 9). These point to an increased influence of the Nile River runoff to the eastern Mediterranean (e.g., Hamann et al., 2009), which is associated with the rainfall in the African Heights (Weldeab et al., 2014; Revel et al., 2015). The Indian Ocean monsoon system causes increased moisture in the Ethiopian Highlands in Africa (e.g., Camberlin, 1997; Tierney et al., 2015). The increased rainfall and consequent Nile inflow shaped the sedimentary regime of the eastern Mediterranean (Fig. 11).

Our data suggest a relative dominance of Nile River sedimentary input during the final stage of the LIA, as compared to the period post LIA. However, data on climatic conditions and rainfall variability over east Africa are scarce for the period from 1750 to the termination of the LIA (e.g., Nicholson, 1998; Nicholson, 2000; Hastenrath, 2001; Hannaford and Beck, 2021). Most documentations record the mid-19th and 20th century (Nicholson et al., 2018 and references therein). Lake Victoria is a sensitive recorder of climate change and together with drainage

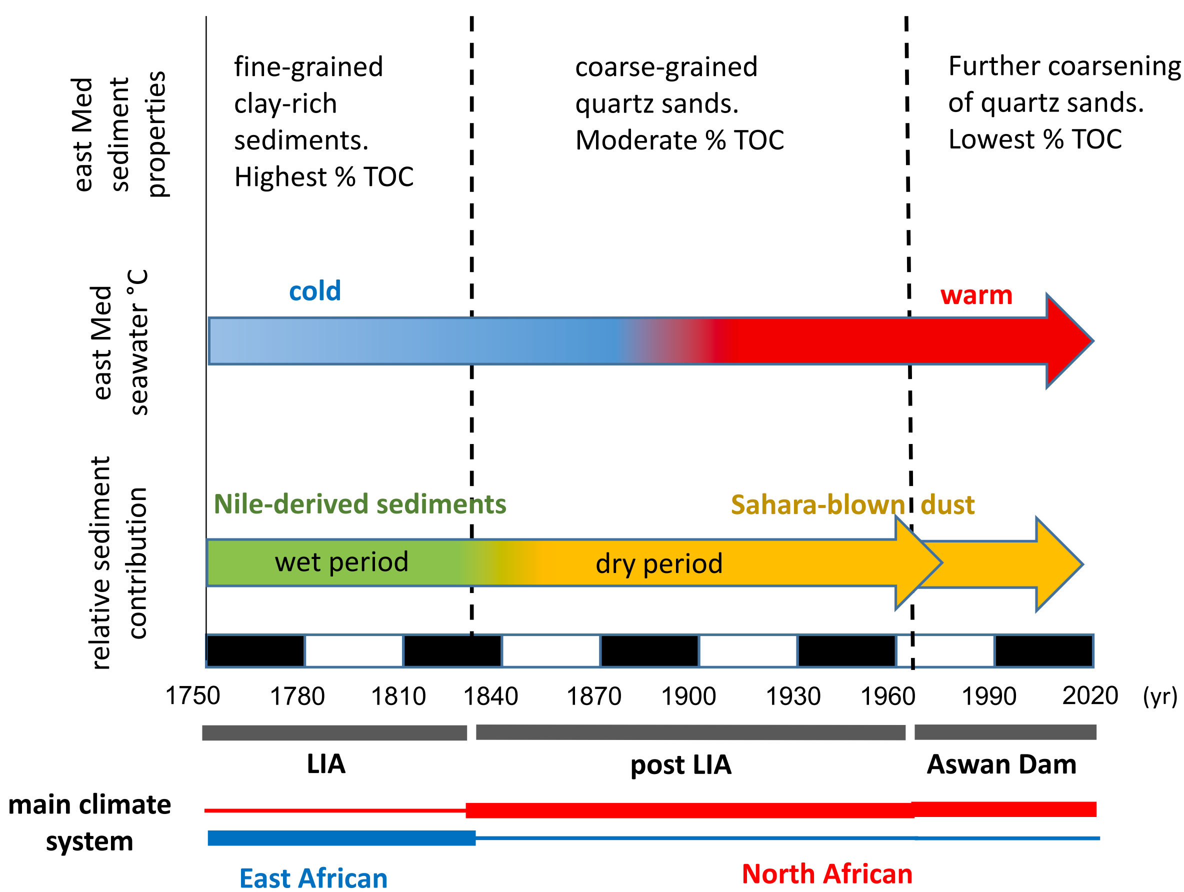

Fig. 11. Schematic diagram showing the main factors influencing the eastern Mediterranean sedimentary regime during the past few hundred years.

from the Ethiopian highlands are the direct source of the Nile River (Garzanti et al., 2015). There is no direct evidence of lake fluctuations prior to 1800 (end of LIA), however, oral traditions and Nile flow evidence indicate a general trend of high lake stand during 1750–1820 associated with wet conditions, a minimum at the termination of the LIA and rising levels from 1830 to 1840 until 1900 (Nicholson, 2000 and references therein; Nicholas et al., 2012; Fig. 8). Additionally, Hastenrath (2001) shows that lake levels in East Africa were high and precipitation was higher prior to 1880, whereas evidence of wetter conditions in the LIA are also shown for southern Africa (Nash et al., 2016; Railsback et al., 2018; Hannaford and Beck, 2021). Wetter conditions in coastal East Africa were shown to have occurred during the LIA by Tierney and others (2015).

The period of the LIA recorded in the studied core is also characterized by lower abundances of miliolid foraminifera compared to post-LIA (Fig. 8). Miliolids secrete imperforate shells of high magnesium calcite, which are most easily produced in warm, shallow waters saturated with $CaCO_3$ (Haynes, 1981). Their small numbers as compared to the period after the LIA are in agreement with colder waters on the seafloor of the eastern Mediterranean during the LIA. That deep waters were colder during the LIA in the eastern Mediterranean has been inferred using planktonic foraminifera (Mojtahid et al., 2015). The climatic conditions during the period corresponding to 1750–1830 over Europe show cold and harsh winters (e.g., PAGES 2k Consortium, 2013). Global climate modeling showed that a southward shift in the tropical rain belt occurs when there is cooling over the northern hemisphere (Hwang et al., 2013). A southern shift in the ITCZ during the LIA is in accordance with cooling in the northern hemisphere at that time (Lechleitner et al., 2017; Railsback et al., 2018 and references therein). In addition, cooling during the LIA is also shown for pollen from coastal Syria (Kaniewski et al., 2011) and is coherent with cooler eastern Mediterranean waters inferred from the small abundances of miliolids in our core.

The termination of the Little Ice Age at 1830 is reflected by a significant change noted in our data. Coral archives from the Indian, western Pacific, and Atlantic oceans also indicate a significant change of a warming trend around 1830–1840 (Tierney et al., 2015). Nicholson (2001) show reduced rainfall conditions in 1820–1830, and (Felis et al., 2000) show a change at that time in coral $\delta^{18}O$ record from the northern Red Sea.

The period following the LIA (1830–2018) is characterized by a constant increase in grain size, a relative increase in quartzose and carbonate material and in K_2O levels, along with a relative decrease in finer aluminosilicate sediments and in %TOC (Figs. 3–6, 9). The relative increase in quartz and calcite may be interpreted as resulting from the decreasing dilution by finer sediments from the Nile River, rather than an absolute quartzose-carbonate increase. However, this change may also point to a shift in the dominant climatic system influencing the sedimentary regime around the eastern Mediterranean. An increasing influence of Saharan dust storms and Saharan sand contribution that are associated with the North African climate system are suggested for this period (Goudie and Middleton, 2001; Hamann et al., 2009). Additionally, significant increase in miliolid abundance (Fig. 8) is in accordance with increased abundances associated with warmer waters.

It seems that variations in the climatic systems over East and North Africa played a fundamental role in shaping the sedimentary record of the eastern Mediterranean during the past two centuries. Saharan/North African dust storms are most common over the eastern Mediterranean (e.g., Ganor and Mamane, 1982; Ganor, 1991; Goudie and Middleton, 2001; Dayan et al., 2008; Hamann et al., 2009). Our results are in agreement with increased dust transport from North Africa across to the eastern Mediterranean post the LIA (Figs. 10 and 11). An increase in Saharan dust events and deposition were also documented from the beginning of the nineteenth century in the Sahel and western Europe regions (Mulitza et al., 2010; Clifford et al., 2019). An arid Sahara is correlated with the ITCZ northwards migration after 1820 (Lechleitner et al., 2017) and Asian monsoon strengthening after the LIA (see Felis et al., 2018).

The period from approximately 1960 in our data, points to an additional increase in relative quartz concentrations together with a rapid decline in phyllosilicates and %TOC (Figs. 4 and 5), increasing rate of grain coarsening (Fig. 3) and lower ferro-aluminous ratio and trace elements (Fig. 6). Also, a significant increase in benthic foraminifera species richness and numerical abundance at 17 cm in the core (Fig. 7), correspond to approximately 1960.

The construction of the Aswan High Dam in 1964 terminated sediment and organic matter inflow from the Nile River (e.g., Krom et al., 1999; Bookman et al., 2021). This most probably resulted in the additional coarsening of sediment grain size and increasing rate of change, as well as the lower concentrations of TOC seen in our core. However, unlike prior studies that associated the coarsening of the sediments in the eastern Mediterranean directly to the construction of the Aswan Dam (Almogi-Labin et al., 2012; Avnaim-Katav et al., 2020, 2021; Bookman et al., 2021; Herut et al., 2023; Katz et al., 2024), our data points to sediment coarsening trend starting after the LIA (Fig. 3), which was well before the construction of the dam. The damming of the Nile River created a further coarsening, superimposed on the existing coarsening trend. Sediment coarsening at 60 m water depth does not seem to reflect increased water energy or periodical decrease in Nile discharge as suggested for shallower water depths from the eastern Mediterranean (Bookman et al., 2021), but rather an additional change in the climatic regime influencing the eastern Mediterranean (Fig. 11). In addition to the decrease in river input, model projections show climate variability in the Mediterranean region, with evidence of a strong drying trend starting in the early 1960s with lowest precipitation rates in the late 1990s (Lelieveld et al., 2012). This would have also influenced the sedimentary regime.

5. Conclusions

We used an array of chemical, sedimentological and micropaleontological records to track recent climatic and ecological events recorded in eastern Mediterranean shelf sediments. By studying the high-resolution record, we could differentiate between natural and anthropogenic influence during the past ~270 years and pinpoint major events.

The grain size, mineralogical and geochemical data indicate a significant shift in sediment sources at the end of the LIA (~1830). During the LIA, coarse quartzose sand was a relatively minor component of the sediments, with a constant amount of about 5%. Following the end of the LIA, the coarse quartzose component increased, reaching modern values of >20%. A further increase in the coarse quartzose component following the Nile damming in the 1960s is superimposed on the preceding post-LIA increase. The geochemical data also indicates a change in the finer-grained component at the end of the LIA. The LIA clay-rich sediments are K_2O depleted and Ni enriched compared with the post-LIA sediments. These changes are thought to reflect a shift in the provenance of the east Mediterranean shelf sediment, from dominant Nile-derived sediments and Nile Delta soils during the LIA, toward more Saharan-derived, fine-grained dust and coarse-grained quartzose sands in the post-LIA period. The dominance of Nile-derived sediments is thought to indicate wetter conditions in coastal East Africa during the LIA, as compared with the post-LIA period.

The foraminiferal data show a change at the end of the LIA as well, specifically in major group composition and total abundance and diversity. Decreased abundances of the miliolid shell-type group during the LIA, followed by a significant increase after the LIA are in accordance with a shift to warmer Mediterranean waters post-LIA. Additional increase in foraminiferal species richness and total abundance occurs after the damming of the Nile and is superimposed on the ongoing trend that started after the LIA.

CRediT authorship contribution statement

Yael Edelman-Furstenberg: Conceptualization, Methodology, Validation, Investigation, Writing – original draft, Project administration, Funding acquisition. **Navot Morag:** Conceptualization, Investigation, Writing – original draft. **Henko C. de Stigter:** Writing – review & editing, Investigation, Validation. **Onn Crouvi:** Validation, Investigation, Writing – review & editing. **Nadya Teutsch:** Validation, Resources. **Orit Hyams-Kaphzan:** Validation, Investigation, Writing – review & editing.

Declaration of competing interest

The authors declare that they have no known competing financial interests or personal relationships that could have appeared to influence the work reported in this paper.

Acknowledgement

We thank the reviewers for their useful suggestions and time put into the review. This research was supported by the Israel Ministry of Energy and Infrastructure grant and by the Geological Survey of Israel.

Appendix A. Supplementary data

Supplementary data to this article can be found online at https://doi.org/10.1016/j.quascirev.2025.109185.

Data availability

All data and/or code is contained within the submission.

References

Abdelsalam, M.G., Liegeois, J.-P., Stern, R.J., 2002. The saharan metacraton. J. Afr. Earth Sci. 34, 119–136, 2002.
Abu Khatita, A.M., 2011. Assessment of soil and sediment contamination in the Middle Nile Delta area (Egypt)-Geo-Environmental study using combined sedimentological, geophysical and geochemical methods. Friedrich-Alexander-Universitaet Erlangen-Nuernberg (Germany) 214. Ph.D. Thesis.
Agiadi, K., Albano, P.G., 2020. Holocene fish assemblages provide baseline data for the rapidly changing eastern Mediterranean. Holocene 30 (10), 1438–1450. .
Almagor, G., Gill, D., Perath, I., 2000. Marine sand resources offshore Israel. Mar. Georesour. Geotechnol. 18 (1), 1–42.
Almogi-Labin, A., Herut, B., Sandler, A., Gelman, F., 2009. Rapid Changes along the Israeli Mediterranean Coast Following the Damming of the Nile and Their Influence on the Israeli Inner Shelf. Geological Survey of Israel, Jerusalem. Report GSI/36/2009; IOLR Report H75/2009. (In Hebrew, with English abstract).
Almogi-Labin, A., Calvo, R., Elyashiv, H., Amit, R., Harlavan, Y., Herut, H., 2012. Sediment Characterization of the Israeli Mediterranean Shelf, p. 38. GSI Report GSI/27/2012 and IOLR Report H68/2012.
Arieli, R.N., Almogi-Labin, A., Abramovich, S., Herut, B., 2011. The effect of thermal pollution on benthic foraminiferal assemblages in the Mediterranean shoreface adjacent to Hadera power plant (Israel). Mar. Pollut. Bull. 62, 1002–1012. https://doi.org/10.1016/j.marpolbul.2011.02.036.
Ashkenazi, L., Katz, O., Abramovich, S., Almogi-Labin, A., Makovsky, Y., Gadol, O., et al., 2022. Benthic foraminifera as indicators of recent mixed turbidite-contourite sediment transport system in the Eastern Mediterranean upper continental slope, offshore Israel. Mar. Geol. 445, 106756. .
Avnaim-Katav, S., Almogi-Labin, A., Schneider-Mor, A., Crouvi, O., Burke, A.A., Kremenetski, K.V., MacDonald, G.M., 2019. A multi-proxy shallow marine record for Mid-to-Late Holocene climate variability, Thera eruptions and cultural change in the Eastern Mediterranean. Quat. Sci. Rev. 204, 133–148. .
Avnaim-Katav, S., Almogi-Labin, A., Kanari, M., Herut, B., 2020. Living benthic foraminifera of southeastern Mediterranean ultra-oligotrophic shelf habitats: implications for ecological studies. Estuar. Coast Shelf Sci. 234, 106633.
Avnaim-Katav, S., Almogi-Labin, A., Herut, B., Kanari, M., Guy-Haim, T., 2021. Benthic foraminifera from the Southeastern Mediterranean shelf: dead assemblages and living-dead comparisons recording consequences of Nile River damming. Mar. Micropaleontol. 164, 101977. .
Bareket, M.M., Bookman, R., Katsman, R., de Stigter, H., Herut, B., 2016. The role of transport processes of particulate mercury in modifying marine anthropogenic secondary sources, the case of Haifa bay, Israel. Mar. Pollut. Bull. 105 (1), 286–291. .
Baskaran, M., 2011. Po-210 and Pb-210 as atmospheric tracers and global atmospheric Pb-210 fallout: a review. J. Environ. Radioact. 102 (5), 500–513. .
Beccaluva, Luigi, Bianchini, Gianluca, Natali, Claudio, Siena, Franca, 2009. Continental flood basalts and mantle plumes: a case study of the Northern Ethiopian Plateau. J. Petrol. 50 (7), 1377–1403.
Biscaye, P.E., 1965. Mineralogy and sedimentation of recent deep-sea clay in the Atlantic Ocean and the adjacent seas and oceans. Geol. Soc. Am. Bull. 76, 803–832.
Bookman, R., Mor-Federman, T., Herut, B., Harlavan, Y., Taha, N., Stein, M., Almogi-Labin, A., 2021. Development of the nile littoral cell during the past 8.2 kyr. Quat. Sci. Rev. 274, 107262. .
Boos, K., Gutow, L., Mundry, R., Franke, H.D., 2010. Sediment preference and burrowing behaviour in the sympatric brittlestars Ophiura albida Forbes, 1839 and Ophiura ophiura (Linnaeus, 1758)(Ophiuroidea, Echinodermata). J. Exp. Mar. Biol. Ecol. 393 (1–2), 176–181. .
Box, M.R., Krom, M.D., Cliff, R.A., Bar-Matthews, M., Almogi-Labin, A., Ayalon, A., Paterne, M., 2011. Response of the Nile and its catchment to millennial-scale climatic change since the LGM from Sr isotopes and major elements of East Mediterranean sediments. Quat. Sci. Rev. 30 (3–4), 431–442. .
Bradley, R.S., Jonest, P.D., 1993. 'Little Ice Age' summer temperature variations: their nature and relevance to recent global warming trends. Holocene 3 (4), 367–376. .
Brenner, I., Watson, A., Russell, G., Goncalves, M., 1980. A new approach to the determination of the major and minor constituents in silicate and phosphate rocks. Chem. Geol. 28, 321–330.
Büntgen, U., Esper, J., Frank, D.C., Nicolussi, K., Schmidhalter, M., 2005. A 1052-year tree-ring proxy for Alpine summer temperatures. Clim. Dynam. 25, 141–153. .
Camberlin, P., 1997. Rainfall anomalies in the source region of the Nile and their connection with the Indian summer monsoon. J. Clim. 10 (6), 1380–1392. .
Clifford, H.M., Spaulding, N.E., Kurbatov, A.V., More, A., Korotkikh, E.V., Sneed, S.B., Handley, M., Maasch, K.A., Loveluck, C.P., Chaplin, J., McCormick, M., Mayewski, P. A., 2019. A 2000 year Saharan dust event proxy record from an ice core in the European Alps. J. Geophys. Res. Atmos. 124 (23), 12882–12900. .
Coll, M., Piroddi, C., Steenbeek, J., Kaschner, K., Lasram, F.B.R., et al., 2010. The biodiversity of the Mediterranean Sea: estimates, patterns, and threats 2011. PLoS One 5, e11842.
Comay, O., Edelman-Furstenberg, Y., Ben-Ami, F., 2015. Patterns in molluscan death assemblages along the Israeli Mediterranean continental shelf. Quat. Int. 390, 21–28.
Cosentino, C., Molisso, F., Scopelliti, G., Caruso, A., Insinga, D.D., Lubritto, C., Pepe, F., Sacchi, M., 2017. Benthic foraminifera as indicators of relative sea-level fluctuations: paleoenvironmental and paleoclimatic reconstruction of a Holocene marine succession (Calabria, south-eastern Tyrrhenian Sea). Quat. Int. 439, 79–101. .
Crouvi, O., Amit, R., Enzel, Y., Porat, N., Sandler, A., 2008. Sand dunes as a major proximal dust source for late Pleistocene loess in the Negev Desert, Israel. Quat. Res. 70 (2), 275–282. https://doi.org/10.1016/j.yqres.2008.04.011.
Crutzen, P.J., 2002. The "anthropocene". J. Phys. IV - Proc. 12 (10), 1–5. EDP sciences.
Dayan, U., Ziv, B., Shoob, T., Enzel, Y., 2008. Suspended dust over South-Eastern Mediterranean and its relation to atmospheric circulations. Int. J. Climatol. 28, 915–924.
de Madron, X.D., Guieu, C., Sempéré, R., Conan, P., Cossa, D., et al., 2011. Marine ecosystems' responses to climatic and anthropogenic forcings in the Mediterranean. Prog. Oceanogr. 91 (2), 97–166. https://doi.org/10.1016/j.pocean.2011.02.003.
Dietl, G.P., Kidwell, S.M., Brenner, M., Burney, D.A., Flessa, K.W., Jackson, S.T., Koch, P. L., 2015. Conservation paleobiology: leveraging knowledge of the past to inform conservation and restoration. Annu. Rev. Earth Planet Sci. 43, 79–103.
Edelman-Furstenberg, Y., Kidwell, S.M., de Stigter, H.C., 2020. Mixing depths and sediment accumulation rates on an arid tropical shelf based on fine-fraction 210Pb analysis. Mar. Geol 425, 106198.
Felis, T., Ionita, M., Rimbu, N., Lohmann, G., Kölling, M., 2018. Mild and arid climate in the eastern sahara-arabian desert during the late little ice age. Geophys. Res. Lett. 45, 7112–7119.
Felis, T., Pätzold, J., Loya, Y., Fine, M., Nawar, A.H., Wefer, G., 2000. A coral oxygen isotope record from the northern Red Sea documenting NAO, ENSO, and North Pacific teleconnections on Middle East climate variability since the year 1750. Paleoceanography 15 (6), 679–694. .
Fishelson, L., 2000. Marine animal assemblages along the littoral of the Israeli Mediterranean seashore: the Red-Mediterranean Seas communities of species. Ital. J. Zool. 67 (4), 393–415. .
Galgani, F., 2015. Marine litter, future prospects for research. Front. Mar. Sci. 2, 87. .
Galil, B.S., Zenetos, A., 2002. A sea change—exotics in the Eastern Mediterranean Sea. Invasive aquatic species of Europe. Distribution, Impacts and Management. , pp. 325–336.
Ganor, E., 1991. The composition of clay minerals transported to Israel as indicators of Saharan dust emission. Atmospheric Environment. Part A. General Topics 25 (12), 2657–2664. .
Ganor, E., Mamane, Y., 1982. Transport of saharan dust across the eastern mediterranean. Atmos. Environ. 16 (3), 581–587, 1967.
Garzanti, E., Andò, S., Padoan, M., Vezzoli, G., El Kammar, A., 2015. The modern Nile sediment system: processes and products. Quat. Sci. Rev. 130, 9–56. .
Garzanti, E., Andò, S., Limonta, M., Fielding, L., Najman, Y., 2018. Diagenetic control on mineralogical suites in sand, silt, and mud (Cenozoic Nile Delta): implications for provenance reconstructions. Earth Sci. Rev. 185, 122–139. .
Gelman, F., Binstock, R., Halicz, L., 2012. Application of the Walkley–Black titration for the organic carbon quantification in organic rich sedimentary rocks. Fuel 96, 608–610.
Glaser, R., Riemann, D., 2009. A thousand-year record of temperature variations for Germany and Central Europe based on documentary data. J. Quat. Sci.: Published for the Quaternary Research Association 24 (5), 437–449. .

Golani, D., 1998. Impact of Red Sea fish migrants through the Suez canal on the aquatic environment of the eastern Mediterranean. Bulletin Series Yale School of Forestry and Environmental Studies 103, 375–387. .
Goudie, A.S., Middleton, N.J., 2001. Saharan dust storms: nature and consequences. Earth Sci. Rev. 56 (1–4), 179–204. .
Grove, J.M., 2001. The initiation of the" little ice age" in regions round the North Atlantic. Climatic Change 48, 53–82.
Halim, Y., Rizkalla, S., Morcos, S.A., El-Sayed, M.K., 1995. The impact of the Nile and the Suez Canal on the living marine resources of the Egyptian Mediterranean waters, 349. , p. 19. Effects of Riverine Inputs on Coastal Ecosystems and Fisheries Resources.
Hamann, Y., Ehrmann, W., Schmiedl, G., Kuhnt, T., 2009. Modern and late Quaternary clay mineral distribution in the area of the SE Mediterranean Sea. Quat. Res. 71 (3), 453–464. .
Hannaford, M.J., Beck, K.K., 2021. Rainfallvariabilityinsoutheastandwest-centralAfrica duringtheLittleIceAge:dodocumentaryandproxy recordsagree? Climatic Change 168, 11, 2021.
Hastenrath, S., 2001. Variations of east climate during the past two centuries. Climatic Change 50, 209–217, 2001.
Haynes, J.R., 1981. Foraminifera. McMIllan, Hong Kong, p. 443.
Hennekam, R., Jilbert, T., Schnetger, B., de Lange, G.J., 2014. Solar forcing of Nile discharge and sapropel S1 formation in the early to middle Holocene eastern Mediterranean. Paleoceanography 29 (5), 343–356. .
Hennekam, Rick, 2015. High-frequency climate variability in the late quaternary eastern mediterranean. Utrecht Stud. Earth Sci N 78.
Herut, B., Almogi-Labin, A., Jannink, N., Gertman, I., 2000. The seasonal dynamics of nutrient and chlorophyll a concentrations on the SE Mediterranean shelf-slope. Oceanol. Acta 23, 771–782. https://doi.org/10.1016/S0399-1784(00)01118-X.
Herut, B., Guy-Haim, T., Almogi-Labin, A., Fischer, H.W., Ransby, D., Sandler, A., Katz, T., Avnaim-Katav, S., 2023. Marine oligotrophication due to fine sediments and nutrient starvation caused by anthropogenic sediment and water retention in large rivers: the Nile damming case. Front. Mar. Sci. 10, 1226379. https://doi.org/10.3389/fmars.2023.1226379.
Hill, J.M., Tyler-Walters, H., 2018. Seapens and burrowing megafauna in circalittoral fine mud. In: Tyler-Walters, H., Hiscock, K. (Eds.), Marine Life Information Network: Biology and Sensitivity Key Information Reviews, [on-Line]. Plymouth: Marine Biological Association of the United Kingdom. https://doi.org/10.17031/marlinhab.131.1.
Hwang, Y.-T., Frierson, D.M.W., Kang, andS.M., 2013. Anthropogenic sulfate aerosol and the southward shift of tropical precipitation in the late20thcentury. Geophys. Res. Lett. 40, 2845–2850.
Hyams-Kaphzan, O., Almogi-Labin, A., Sivan, D., Benjamini, C., 2008. Benthic foraminifera assemblage change along the southeastern Mediterranean inner shelf due to fall-off of Nile-derived siliciclastics. Neues Jahrbuch Geol. Palaontol. Abhand. 248, 315–344.
Hyams-Kaphzan, O., Almogi-Labin, A., Benjamini, C., Herut, B., 2009. Natural oligotrophy vs. pollution-induced eutrophy on the SE Mediterranean shallow shelf (Israel): environmental parameters and benthic foraminifera. Mar. Pol. 58, 1888–1902.
Incarbona, A., Ziveri, P., Di Stefano, E., Lirer, F., Mortyn, G., Patti, B., Pelosi, N., Sprovieri, M., Tranchida, G., Vallefuoco, M., Albertazzi, S., Bellucci, L.G., Bonanno, A., Bonanno, S., Censi, P., Ferraro, L., Giuliani, S., Mazzola, S., Sprovieri, R., 2010. Calcareous nannofossil assemblages from the Central Mediterranean Sea over the last four centuries: the impact of the little ice age. Clim. Past 6, 795–805. .
Kalman, A., Goodman-Tchernov, B., Hill, P., Everhardt IV, C., Mathalon, A., Katz, T., 2022. Anthropogenic changes in waterways produce "drought-like" layers in shelf sediments. Elem Sci Anth 10 (1), 00039. .
Kaniewski, D., Van Campo, E., Paulissen, E., Weiss, H., Bakker, J., Rossignol, I., Van Lerberghe, K., 2011. The medieval climate anomaly and the little Ice Age in coastal Syria inferred from pollen-derived palaeoclimatic patterns. Global Planet. Change 78 (3–4), 178–187.
Katsanevakis, S., Coll, M., Piroddi, C., Steenbeek, J., Ben Rais Lasram, F., Zenetos, A., Cardoso, A.C., 2014. Invading the Mediterranean Sea: biodiversity patterns shaped by human activities. Front. Mar. Sci. 1, 32. .
Katz, T., Crouvi, O., 2018. Sediment flux dynamics over the shallow (25 m depth) shelf of the Mediterranean Sea along the Israeli coast. Mar. Geol. 406, 1–11. .
Katz, T., Bookman, R., Herut, B., Goodman-Tchernov, B., Sisma-Ventura, G., 2024. Far-field effects of the nile damming on the silica cycle in the southeastern Mediterranean Sea. Sci. Total Environ. 921, 171274. .
Kress, N., Herut, B., Galil, B.S., 2004. Sewage sludge impact on sediment quality and benthic assemblages off the Mediterranean coast of Israel-a long-term study. Mar. Environ. Res. 57, 213–233. https://doi.org/10.1016/S0141-1136(03)00081-3.
Kenigsberg, C., Titelboim, D., Ashckenazi-Polivoda, S., Herut, B., Kucera, M., Zukerman, Y., Hyams-Kaphzan, O., Almogi-Labin, A., Abramovich, S., 2022. The combined effects of rising temperature and salinity may halt the future proliferation of symbiont-bearing foraminifera as ecosystem engineers. Sci. Total Environ. 806, 150581. .
Krom, M.D., Cliff, R.A., Eijsink, L.M., Herut, B., Chester, R., 1999. The characterization of Saharan dusts and Nile particulate matter in surface sediments from the Levantine basin using Sr isotopes. Mar. Geol. 155, 319–330.
Lechleitner, F.A., Breitenbach, S.F., Rehfeld, K., Ridley, H.E., Asmerom, Y., Prufer, K.M., Marwan, N., Goswami, B., Kennett, D.J., Aquino, V.V., Polyak, V., Haug, G.H., Eglinton, T.I., Baldini, J.U., 2017. Tropical rainfall over the last two millennia: evidence for a low-latitude hydrologic seesaw. Sci. Rep. 7 (1), 45809. .
Lelieveld, J., Hadjinicolaou, P., Kostopoulou, E., et al., 2012. Climate change and impacts in the eastern mediterranean and the Middle East. Climatic Change 114, 667–687.
Leshno, Y., Edelman-Furstenberg, Y., Mienis, H.K., Benjamini, Ch, 2015. Molluscan live and dead assemblages in an anthropogenically stressed shallow-shelf: Levantine margin of Israel. Palaeogeogr. Palaeoclimatol. Palaeoecol. 433, 49–59.
Lionello, P., Giorgi, F., Rohling, E., Seager, R., 2023. Mediterranean climate: past, present and future. In: Oceanography of the Mediterranean Sea. Elsevier, , pp. 41–91.
Maryol, E., Lin, C., 2015. Geochemical characteristics of soils in Fezzan, Sahara desert: implications for environment and agriculture. J. Geochem. Explor. 158, 122–131. .
Matthews, J.A., Briffa, K.R., 2005. The 'Little Ice Age': re-evaluation of an evolving concept. Geogr. Ann. Phys. Geogr. 87 (1), 17–36. .
Moffa-Sánchez, P., Hall, I.R., Barker, S., Thornalley, D.J., Yashayaev, I., 2014. Surface changes in the eastern labrador sea around the onset of the little ice age. Paleoceanography 29 (3), 160–175. .
Mojtahid, M., Manceau, R., Schiebel, R., Hennekam, R., De Lange, G.J., 2015. Thirteen thousand years of southeastern Mediterranean climate variability inferred from an integrative planktic foraminiferal-based approach. Paleoceanography 30 (4), 402–422. .
Moore, D.M., Reynolds Jr, R.C., 1989. X-Ray Diffraction and the Identification and Analysis of Clay Minerals. Oxford University Press (OUP), .
Moreno, T., Querol, X., Castillo, S., Alastuey, A., Cuevas, E., Herrmann, L., Mounkaila, M., Elvira, J., Gibbons, W., 2006. Geochemical variations in aeolian mineral particles from the Sahara–Sahel dust corridor. Chemosphere 65 (2), 261–270. .
Moshe, N., Katz, O., Torfstein, A., Kanari, M., Masque, P., Hyams-Kaphzan, O., 2024. Glacial-Holocene variability in sediment accumulation and erosion along submarine blind canyons: a case study from Eastern Mediterranean Sea. Mar. Geol. 469, 107217.
Mulitza, S., Heslop, D., Pittauerova, D., Fischer, H.W., Meyer, I., Stuut, J.B., Zabel, M., Mollenhauer, G., Collins, J.A., Kuhnert, H., Schulz, M., 2010. Increase in African dust flux at the onset of commercial agriculture in the Sahel region. Nature 466 (7303), 226–228. .
Murray, J.W., 1973. Distribution and Ecology of Living Benthic Foraminiferids. Heinemann, London.
Nash, D.J., Pribyl, K., Klein, J., et al., 2016. Seasonal rainfall variability in southeast Africa during the nineteenth century reconstructed from documentary sources. Climatic Change 134, 605–619.
Nicholson, S.E., 1998. Historical fluctuations of lake Victoria and other lakes in the northern Rift valley of East Africa. Environmental Change and Response in East African Lakes. , pp. 7–35.
Nicholson, S.E., 2000. The nature of rainfall variability over Africa on time scales of decades to millennia. Global Planet. Change 26, 137–158.
Nicholson, S.E., 2001. Climatic and environmental change in Africa during the last two centuries. Clim. Res. 17 (2), 123–144. .
Nicholson, S.E., Funk, C., Fink, A.H., 2018. Rainfall over the African continent from the 19th through the 21st century. Global Planet. Change 165, 114–127. .
Nir, Y., 1984. Recent sediments of the Israel Mediterranean continental shelf and slope. Ph.D. Thesis, Department of Marine Geology. University of Goteborg.
Nixon, S.W., 2003. Replacing the Nile: are anthropogenic nutrients providing the fertility once brought to the Mediterranean by a great river? Ambio 32 (1), 30–39.
PAGES 2k Consortium, 2013. Continental-scale temperature variability during the past two millennia. Nat. Geosci. 6, 339–346.
Pasternak, G., Ribic, C.A., Spanier, E., Ariel, A., Mayzel, B., Ohayon, S., Zviely, D., 2019. Nearshore survey and cleanup of benthic marine debris using citizen science divers along the Mediterranean coast of Israel. Ocean Coast Manag. 175, 17–32. .
Perner, K., Moros, M., Jennings, A., Lloyd, J.M., Knudsen, K.L., 2013. Holocene palaeoceanographic evolution off West Greenland. Holocene 23 (3), 374–387. .
Por, F.D., 1989. The Legacy of Tethys: an Aquatic Biogeography of the Levant. Kluwer Academic Publishers, The Netherlands, p. 214.
Railsback, L.B., Brook, G.A., Liang, F., Voarintsoa, N.G., Cheng, H., Edwards, R.L., 2018. A multi-proxy climate record from a northwestern Botswana stalagmite suggesting wetness late in the Little Ice Age (1810–1820 CE) and drying thereafter in response to changing migration of the tropical rain belt or ITCZ. Palaeogeogr. Palaeoclimatol. Palaeoecol. 506, 139–153.
Revel, M., Ducassou, E., Skonieczny, C., Colin, C., Bastian, L., Bosch, D., Migeon, S., Mascle, J., 2015. 20,000 years of Nile River dynamics and environmental changes in the Nile catchment area as inferred from Nile upper continental slope sediments. Quat. Sci. Rev. 130, 200–221.
Rilov, G., Galil, B.S., 2009. Marine bioinvasions in the Mediterranean Sea – history, distribution and ecology. In: Rilov, G., Crooks, J.A. (Eds.), Biological Invasions in Marine Ecosystems: Ecological, Management and Geographic Perspectives. Springer-Verlag, Berlin, pp. 549–575.
Rosentraub, Z., Brenner, S., 2007. Circulation over the southeastern continental shelf and slope of the Mediterranean Sea: direct current measurements, winds, and numerical model simulations. J. Geophys. Res. 112, C11001. https://doi.org/10.1029/2006JC003775.
Sandler, A., 2013. Clay distribution over the landscape of Israel: from the hyper-arid to the Mediterranean climate regimes. Catena 110, 119–132.
Sandler, A., Meunier, A., Velde, B., 2015. Mineralogical and chemical variability of mountain red/brown Mediterranean soils. Geoderma 239, 156–167. .
Sandler, A., Herut, B., 2000. Composition of clays along the continental shelf off Israel: contribution of the Nile versus local sources. Mar. Geol. 167 (3–4), 339–354. .
Schattner, U., 2021. Isolating the role of shore-parallel sediment transport in continental shelf build-up. Continent. Shelf Res. 225, 104480. .

Schilman, B., Almogi-Labin, A., Bar-Matthews, M., Labeyrie, L., Paterne, M., Luz, B., 2001. Long- and short-term carbon fluctuations in the Eastern Mediterranean during the late Holocene. Geology 29, 1099–1102. https://doi.org/10.1130/0091-7613(2001)029.

Stanley, J., 1988. Low sediment accumulation rates and erosion on the middle and outer Nile delta shelf off Egypt. Mar. Geol. 84 (1–2), 111–117.

Stanley, D.J., 1989. Sediment transport on the coast and shelf between the Nile Delta and Israeli margin as determined by heavy minerals. J. Coast Res. 813–828. .

Tapiero, I., 2002. High Resolution Paleoecologic and Paleoclimatic Changes of the Holocene, Based on Benthic Foraminifera and Sediments from the Mediterranean Inner Shelf, Israel. MSc Thesis. Ben-Gurion University of the Negev, BeerSheva, Israel, p. 130 (In Hebrew, English abstract).

Tierney, J.E., Abram, N.J., Anchukaitis, K.J., Evans, M.N., Giry, C., Kilbourne, K.H., Saenger, C.P., Wu, H.C., Zinke, andJ., 2015. Tropical seasurface temperatures for the past four centuries reconstructed from coral archives. Paleoceanography 30, 226–252.

Titelboim, D., Almogi-Labin, A., Herut, B., Kucera, M., Schmidt, C., Hyams-Kaphzan, O., Ovadia, O., Abramovich, S., 2016. Selective responses of benthic foraminifera to thermal pollution. Mar. Pollut. Bull. 105 (1), 324–336.

Weldeab, S., Menke, V., Schmiedl, G., 2014. The pace of East African monsoon evolution during the Holocene. Geophys. Res. Lett. 41, 1724–1731.

Yu, Z., Robinson, P., McGoldrick, P., 2001. An evaluation of methods for the chemical decomposition of geological materials for trace element determination using ICP-MS. Geostand. Geoanal. Res. 25, 199–217.

Zalasiewicz, J., Waters, C.N., Ellis, E.C., Head, M.J., Vidas, D., Steffen, W., et al., 2021. The Anthropocene: comparing its meaning in geology (chronostratigraphy) with conceptual approaches arising in other disciplines. Earth's Future 9, e2020EF001896. https://doi.org/10.1029/2020EF001896.

Zviely, D., Kit, E., Klein, M., 2007. Longshore sand transport estimates along the Mediterranean coast of Israel in the Holocene. Mar. Geol. 238, 61–73.